Materials Science in Semiconductor Processing 84 (2018) 138–143

Contents lists available at ScienceDirect

Materials Science in Semiconductor Processing

journal homepage: www.elsevier.com/locate/mssp

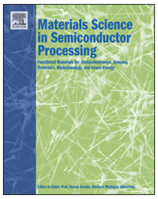

Large-grained Sb_2S_3 thin films with Sn-doping by chemical bath deposition for planar heterojunction solar cells

U. Chalapathi, B. Poornaprakash, Chang-Hoi Ahn, Si-Hyun Park*

Department of Electronic Engineering, Yeungnam University, Gyeongsan 38541, South Korea

ARTICLE INFO

Keywords:
Sb_2S_3 thin films
Sn doping
Chemical bath deposition
Annealing
Structural properties
Electrical properties

ABSTRACT

Herein, the growth of large-grained and compact Sb_2S_3 thin films with good electrical properties by Sn doping using a chemical bath deposition (CBD) and annealing approach is detailed. Sn-doped Sb_2S_3 thin films were prepared using the CBD method with $SbCl_3$, $SnCl_2.2H_2O$, and $Na_2S_2O_3$ as source materials, and ethylenediamine tetraacetic acid (EDTA) as the complexing agent at 40 ° C for 3 h followed by annealing at 250 °C for 30 min under Ar ambience. Un-doped Sb_2S_3 films exhibited an orthorhombic crystal structure with lattice parameters of $a = 1.142$ nm, $b = 0.381$ nm, and $c = 1.124$ nm, crystalline grain sizes of 100 nm, a direct optical band gap of 1.70 eV, p-type electrical conductivity with high electrical resistivity, and low hole mobility. With Sn doping, a significant increase in the grain size of the films from 6 to >10 μm was observed with increasing Sn content from 1.0 to 5.5 at% followed by a decrease in the grain size. The direct optical band gap of the films was 1.71–1.72 eV. By varying Sn at%, the electrical resistivity of the films decreased, and hole mobility increased from 117 to 205 $cm^2\,V^{-1}\,s^{-1}$ up to 5.5 at% and decreased to 166 $cm^2\,V^{-1}\,s^{-1}$ at 7.2 at%. With the addition of 1.0–5.5 at% Sn in the Sb_2S_3 films, the grain growth and electrical properties of the films were drastically enhanced, which is beneficial for the fabrication of planar heterojunction solar cells.

1. Introduction

Sb_2S_3 has gained significant interest in recent years because of its excellent optoelectronic properties which are suited for solar cells, photodetectors, microwave devices, and thermoelectric devices. Sb_2S_3 exhibits distinct properties including a direct optical band gap of 1.7 eV, high optical absorption coefficient, and simple processing with stable and abundant constituent elements. Furthermore, Sb_2S_3-based solar cells have exhibited very good performance to date, making Sb_2S_3 a promising solar cell material for further development. Two architectures are generally used in Sb_2S_3-based solar cells: *meso*superstructured (MS) and planar-heterojunction (PHJ). MS devices consist of a metal-oxide (such as TiO_2, Al_2O_3) scaffold infiltrated with Sb_2S_3 [1,2]. The basic structure of PHJ solar cells consist of a Sb_2S_3 material sandwiched between a hole transport material (HTM) and an electron transport material (ETM) with contact electrodes on both sides. Upon the absorption of incident photons, carriers are generated in the absorber, and travel through the ETM and HTM to reach the electrodes. Although, excellent efficiencies have been obtained in MS device [3,4], homogeneous infiltration of the Sb_2S_3 precursor remains an issue [2]. The PHJ structure prevents the pore filling and simplifies the device fabrication process without sacrificing efficiency [5,6]. Moreover, the PHJ device structure is simple and can be formed with low processing temperature, low power consumption, and the possibility for roll-to-roll manufacturing on flexible substrates. In addition, the Sb_2S_3-based solar cells fabricated with PHJ structure exhibit a maximum efficiency of 4.3% [6]. Compared to the maximum efficiency of 7.5% in MS devices, the efficiency of the PHJ device (4.3%) for Sb_2S_3-based solar cells has room for improvement.

Escorcia-Garcia et al. [7] reported a Sb_2S_3-based PHJ solar cell with a conversion efficiency of 1.27% using films prepared by evaporation. Yuan et al. [5] reported Sb_2S_3-based PHJ solar cells with a conversion efficiency of 3.5% using films prepared with large grains and preferred orientations. Wang et al. [6] reported Sb_2S_3-based PHJ solar cells with an efficiency of 4.3% using large-grained Sb_2S_3 thin films fabricated by a fast-chemical approach. These studies indicated that the production of large-grained Sb_2S_3 thin films is essential to further improve the device performance. Ito et al. [8] studied the doping effects in a Sb_2S_3 absorber by chemical bath deposition (CBD), and the full-inorganic solar cell based on an optimized Ti-doped Sb_2S_3 absorber reached a power conversion efficiency (PCE) of 5.7%. Cardenas et al. [9] reported improved electrical properties of Sb_2S_3 thin films by carbon doping. Mustaq et al. [10,11] reported an increase in the grain size of Sb_2S_3 thin films with Sn doping, which motivated us to improve the grain size of Sb_2S_3 thin films

---

* Corresponding author.
E-mail address: sihyun_park@ynu.ac.kr (S.-H. Park).

https://doi.org/10.1016/j.mssp.2018.05.017
Received 11 March 2018; Received in revised form 11 May 2018; Accepted 15 May 2018

by doping. We have used Sn as a dopant for the Sb_2S_3 because Sn^{4+} ion has a standard ionic radius of 0.71 Å, which is slightly less than that of Sb^{3+} (0.76 Å), we expect that Sn ions substitute Sb ions in the Sb_2S_3 crystalline structure. Thus, Sn-doping is expected to be substitutional on the Sb site and hence is expected to be an acceptor. A simple and inexpensive CBD technique followed by annealing was used to grow Sn-doped Sb_2S_3 thin films. The films exhibited compact and large grain sizes of 6–10 μm with good electrical properties.

2. Materials and methods

Un-doped and Sn-doped Sb_2S_3 thin films (1.0–7.2 at%) were prepared via CBD followed by annealing. $SbCl_3$ was used as the Sb source, $Na_2S_2O_3$ as the S source, $SnCl_2.2H_2O$ as the Sn source, and ethylenediamine tetraacetic acid (EDTA) as the complexing agent in the starting solution. Prior to deposition, soda-lime substrates were chemically cleaned and rinsed with deionized water, and dried with nitrogen. The deposition method for pure Sb_2S_3 film growth involved mixing 2.28 g of $SbCl_3$ in 5 mL of acetone, 2.5 mL of 0.5 M EDTA, 20 mL of 1 M $Na_2S_2O_3$, and the required amount of deionized water, to prepare a 100 mL solution. For Sn doping, appropriate amounts of $SbCl_3$ and $SnCl_2.2H_2O$ were dissolved in 5 mL of acetone, 2.5 mL of 0.5 M EDTA, 20 mL of 1 M $Na_2S_2O_3$, and the required amount of deionized water, to prepare a 100 mL solution. The bath temperature was maintained at 40 °C, where the beaker containing this solution was placed. The chemically cleaned soda-lime glass substrates were also placed into this solution and deposition was allowed to proceed for 3 h. After deposition, the samples were removed from the bath, washed with deionized water, and dried with N_2. The films were then subjected to annealing at 250 °C for 30 min in a single-zone quartz tubular furnace by keeping the samples in a graphite box and filling with Ar gas to atmospheric pressure.

Glancing incident X-ray diffraction (GIXRD) patterns of the films were acquired using an X-ray diffractometer (PANalytical) and Cu K_α radiation ($\lambda = 0.15406$ nm) at a glancing angle (ω) of 3°. Raman spectra were recorded using a confocal Raman spectrometer (Thermo Fisher Scientific, Nicolet 6700) with a 532 nm laser source. The morphology and thickness of the films were determined using field emission scanning electron microscope (FESEM, Hitachi, S-4100). The elemental composition of the films was determined using energy-dispersive X-ray spectroscopy (EDS) coupled with FESEM. The transmittance curves of the films were recorded with a UV–Vis–NIR double beam spectrophotometer (Cary 5000). The electrical properties of the films were measured using an EUCOPIA Hall measurement unit (HMS-3000).

3. Results and discussion

Table 1 lists the elemental composition of the Sb_2S_3 thin films prepared with various Sn at%. The un-doped Sb_2S_3 films showed a Sb-rich and S-poor composition. Upon increasing the Sn doping from 1.0 to 7.2 at%, a corresponding decrease in Sb at% was observed. Overall, the elemental composition of the films is metal-rich and S-poor, considering the accuracy limits of EDS analysis.

Table 1
Elemental composition of the Sn-doped Sb_2S_3 films with various dopant concentrations.

S.No	Atomic percentage		
	Sb	S	Sn
1	46.4	53.6	0.0
2	45.7	53.3	1.0
3	43.4	54.5	2.1
4	42.3	53.7	4.3
5	41.5	54.0	5.5
6	38.5	54.3	7.2

The surface morphologies of the un-doped and Sn-doped Sb_2S_3 thin films were observed by FESEM and are shown in Fig. 1. The FESEM image of the un-doped Sb_2S_3 film shows the formation of compact film and uniform distribution of fine grains over the surface. The doping of 1 at% Sn in the films resulted in the formation of 6 μm grains with clearly visible grain boundaries. Many fine grains covering these large grains could also be resolved on the film surface. These large-grain formations are solely due to the incorporation of Sn in the films. Upon increasing the extent of Sn doping from 2.0 to 5.5 at%, the grain size reached >10 μm with the fine grains still present on the surface. Further increasing the Sn doping to 7.2 at% resulted in the disappearance of grain boundaries and clustering of grains on the surface. The grain sizes reported in a previous study of Sn-doped Sb_2S_3 films by Mushtaq et al. [11] were limited to 1.0 μm. The grain sizes obtained in this study are nearly equal to those reported by Wang et al. [6] who used a spin coating and annealing approach. The possible reason for obtaining large-grained Sb_2S_3 films compared to the reported work [10,11] could be due to annealing the films at atmospheric Ar pressure for a duration of 30 min. However, Mustaq et al. [10,11] annealed the Sn-doped Sb_2S_3 films under vacuum for a longer duration of 2 h and obtained 1.0 μm grained films; the longer annealing duration and vacuum annealing could be the possible reasons for the small grain growth. This study clearly reveals that a Sn content from 1.0 to 5.5 at% and a short annealing duration of 30 min at 250 °C under atmospheric Ar pressure are required to obtain large-grained, compact and good-quality Sb_2S_3 films.

Cross-sectional FESEM images were also recorded to observe the effect of Sn doping on the film growth and are shown in Fig. 2. From the cross-sectional image of the un-doped Sb_2S_3 film, it is clear that a compact film was formed with fine particles distributed throughout its thickness. The crystallinity of the un-doped film was determined to be poor. From the cross-sectional image of the film doped with 1 at% Sn, the compactness, crystallinity, and grain sizes increase uniformly. However, the grain size in the cross-section differ from the 6 μm observed at its surface, indicating that the growth of large grains is restricted to the surface of the film. This also clearly indicates the improvement of crystallinity in the films with 1 at% Sn doping. In the cross-sectional images of the films prepared with increased Sn doping from 2.0 to 7.2 at%, a slight decrease in film thickness from 0.7 to 0.5 μm was observed, but its crystallinity, and compactness were retained. Overall, there is a clear change in the crystallinity of the Sb_2S_3 films upon Sn doping.

Elemental mapping by EDS was recorded for a typical 2.0 at% Sn-doped Sb_2S_3 sample to see the distribution of Sb, S and Sn over the film, which is shown in Fig. 3. From the EDS elemental mapping, it is clear that the Sb, S, and Sn are evenly distributed over the entire substrate.

Fig. 4 shows the X-ray diffraction patterns of the un-doped and Sn-doped Sb_2S_3 thin films. A standard stick pattern corresponding to pure Sb_2S_3 (JCPDS card no. 42-1393) is included in the diffraction patterns to clearly evaluate the phase formations in the films with Sn doping. The XRD pattern of the un-doped Sb_2S_3 film exhibited an intense peak at 24.96° and low intensity peaks at positions matching the standard stick pattern of Sb_2S_3. The films exhibited orthorhombic crystal structure with (130) as the preferred orientation. The lattice parameters of the films were $a = 1.142$ nm, $b = 0.381$ nm, and $c = 1.124$ nm, which are similar to the reported values of Sb_2S_3. In the XRD patterns of the Sn-doped Sb_2S_3 films, no noticeable change in peak positions was observed upon increasing Sn dopant concentration. However, the intensity of the (211) peak slightly increased and became dominant for the films doped with 5.5 at% Sn. Further increase in the Sn concentration to 7.2 at% resulted in the (020) and (130) peaks becoming dominant. This indicates a change in the growth direction of Sb_2S_3 from the (130) plane to (230) plane with 5.5 at% of Sn to (020) and (130) directions with 7.2 at% Sn doping. Mushtaq et al. [11] observed a similar change in the growth direction with Sn doping.

The micro-Raman spectra for the un-doped and Sn-doped Sb_2S_3 films were recorded for phase analysis. Fig. 5 shows the Raman spectra